# Modeling Charge Transfer in Oxidized Bacterial Antenna Complexes

**Dmitri Kolbasov,[†] Nagarajan Srivatsan,[†,‡] Nina Ponomarenko,[†] Martin Jäger,[†] and James R. Norris, Jr.*[,†,§]**

*Department of Chemistry, University of Chicago, 5735 South Ellis Avenue, Chicago, Illinois 60637, and Institute of Biodynamics, University of Chicago, 5735 South Ellis Avenue, Chicago, Illinois 60637*

*Received: July 11, 2002; In Final Form: December 16, 2002*

Bacterial light harvesting complexes type 1, LH1, probably contain a circular array of about 32 bacteriochlorophyll (BChl) pigments at a center-to-center distance of about 1 nm. Upon treatment with potassium ferricyanide, some of the BChls are reversibly oxidized, thus forming holes. The measured electron paramagnetic resonance (EPR) spectra of oxidized, detergent-isolated LH1 complexes from *Rhodobacter sphaeroides* and membrane-bound LH1 complexes from *Blastochloris* (formerly *Rhodoseudomonas*) *viridis* at 300 K have the width of 0.45 and 0.35 mT, respectively. This line width is independent of the fraction of the pigments oxidized, at least in the range of 3−30%. The EPR spectra of LH1 are 3−4 times as narrow as those of the monomer BChl cation, which is the evidence for the spin diffusion. The diffusion of holes in LH1 is simulated including electron transfer, mutual spin−spin repulsion, and spin exchange. A method for calculating the EPR spectrum from the simulated trajectories is described providing an opportunity to calculate the EPR spectrum of interacting, moving charges in a highly confined region. The observed spectral line width corresponds to an electron transfer rate constant in the range of $10^8-10^9$ $s^{-1}$. The calculated EPR line width weakly depends on the fraction of pigments oxidized in the range of 0−0.40 assuming strong Heisenberg spin exchange accompanied by electron transfer.

## Introduction

Antennae of photosynthetic bacteria are the pigment−protein complexes that absorb light and efficiently transport the excitation energy to the reaction center (RC) where this energy is used for charge separation.[1−5] Photosynthetic purple bacteria can possess two types of antenna (light-harvesting) complexes, LH1 and LH2. Structural data for LH1 and LH1 RC core complexes have been obtained from electron microscopy investigations that indicate that the basic LH1 unit contains two bacteriochlorophyll (BChl) pigments and about 16 units form either a partial or a complete ring around the RC.[6−13] After they are oxidized with potassium ferricyanide, LH1 complexes exhibit electron paramagnetic resonance (EPR) signals. Such signals have been observed earlier for oxidized detergent-isolated and membrane-bound LH1 systems from *Rhodospirillum rubrum*, *Rhodobacter sphaeroides*, *Ectothiorhodospira sphaeroides*, and *Rhodobacter capsulatus*.[14−17] The EPR line widths were about 0.4 mT in all cases, which is significantly smaller than the 1.35 mT width of the monomer BChl *a* cation in organic solvents. The formation of the EPR signal was correlated with the bleaching of the absorption band of LH1. This EPR signal from LH1 has been assigned to radical cations of BChl, narrowed by fast charge transfer over the ring of BChl molecules. According to the special pair model, which can be applied in the case of very fast electron transfer, for Gaussian monomer and *N*-mer spectra, the peak-to-peak line widths are related as $\Delta H_N = \Delta H_M/N^{1/2}$.[18] This model, being used to explain the 0.4 mT wide line, predicts that LH1 contains 12 BChls or 6 $\alpha\beta(BChl)_2$ units.[14−17] However, this interpretation seems inconsistent with the structural information that is now available for LH1 that indicates a much larger number of BChls than 12. Another possibility, the one explored in this paper, is that the charge delocalization process in LH1 is rate-limited, such that each spin is effectively delocalized over only a limited number of BChls and not over all BChls of the LH1 complex. In this case, the EPR line width reflects the electron transfer rate constant rather than the aggregation size.

The structure for LH1 obtained by computational modeling indicates BChl*a* Mg−Mg separations of about 1 nm[19] for which the electron transfer should occur on the nanosecond time scale.[20,21] Thus, hole transfer in LH1 is particularly convenient for study by means of EPR. Although the pigment structure of antennae is most likely optimized for efficient energy transfer, no light-induced charge transfer occurs in vivo. However, when the BChls of the antennae are chemically oxidized to form radical cations, antennae might serve as circular-like charge conductors. In many respects, the oxidized antennae represent a unique system, since no other natural structures are known to contain such long arrays of densely packed, ordered pigments. Because no preferential direction exists in antennae, the charge transfer is assumed to be a random walk process. The other mechanism, which also may cause narrowing of the EPR spectrum, is Heisenberg spin exchange,[22] a bimolecular process with increasing significance as the number of holes increase. Experimentally, we have measured the room temperature EPR spectra of the detergent-isolated LH1 complexes of *R. sphaeroides* and the LH1 of photosynthetic membranes from *Blastochloris* (formerly *Rhodopseudomonas*[23]) *viridis* treated with various amounts of oxidant. Computer simulations of the spin dynamics

* To whom correspondence should be addressed. Tel: (773)702-7864. Fax: (773)702-9646. E-mail: j-norris@uchicago.edu.
† Department of Chemistry, University of Chicago.
‡ Present address: Division of Chemistry and Chemical Engineering, Mail Stop 127-72, California Institute of Technology, Pasadena, California 91125.
§ Institute of Biodynamics, University of Chicago.

10.1021/jp0265079 CCC: $25.00 
Published on Web 02/14/2003

in antennae have been performed, and the corresponding EPR spectra have been calculated and compared to experiment. The aim of this work is to determine the rates of the hole transfer and spin exchange based on the EPR spectra of the oxidized bacterial antennae.

## Experimental Section

**Preparation of Photosynthetic Membranes.** For preparation of membranes from *B. viridis*, the photoheterotrophically grown cells of *B. viridis* (ATCC 19567) were suspended in 10 mM Tris-HCl buffer, pH 7.8, containing 0.01 mM ethylenediaminetetraacetic acid. Cells were disrupted with sonication using a temperature-regulated Cole Parmer Ultrasonic Homogenizer (~90% amplitude, 2.5 s on/2.5 s off cycle, ~8 °C). Cell debris was removed by low speed centrifugation at 2000*g* at 4 °C for 15 min in a Sorvall RC-5B centrifuge. Intracytoplasmic membranes were sedimented at 146 000*g* for 1 h using a Beckman LE-80 Preparative Ultracentrifuge with a fixed angle rotor. Membranes containing photosynthetic proteins were purified by sucrose density gradients (1.12−1.22 kg $L^{-1}$) (Hoefer S100 gradient maker) spun at 184 000*g* at 4 °C. The photosynthetic membranes were collected from bands that equilibrated at 1.14−1.15 kg $L^{-1}$, washed twice, and resuspended in buffer solution. Isolation of LH1 complex from *R. sphaeroides* was described previously.[24]

**Generation of Radical Cations and Visible Absorption Spectroscopy.** Radical cations were generated in the samples by oxidation with potassium ferricyanide. We used fresh membrane preparations from *B. viridis*, whereas suspensions of LH1 complexes from *R. sphaeroides* had been kept frozen before being used. A few microliters of the freshly prepared oxidant solution were added to 400 $\mu$L of the sample suspension. Then, the samples were vortexed for 10 s and transferred to a 1 mm path length quartz cuvette for the VIS absorption measurement. After this measurement, the samples were transferred to a quartz EPR flat cell. For low temperature measurements, the samples were transferred to cylindrical quartz EPR tubes and frozen in liquid nitrogen. The optical densities at the absorption maximum (~880 nm for *R. sphaeroides* and ~1015 nm for *B. viridis*) of all samples prior to oxidation were close to 25 $cm^{-1}$. Optical absorption spectra were measured with a Shimadzu UV-1601 spectrophotometer. The fraction of LH1 BChls oxidized, $\chi$, was determined from the extent to which the near-infrared absorption band of the antenna was bleached. Prior to calculating $\chi$, the absorbances were corrected for changes caused by dilution.

**EPR Measurements.** The EPR spectra were taken immediately after the oxidation of the samples. Spectra were recorded on a Varian E-Line magnet system. Samples were measured in a Varian TE102 cavity attached to a Bruker ER041MR microwave bridge operating at X-Band. The raw signal was amplified by a Hewlett-Packard 461A amplifier. Phase sensitive detection at 100 kHz field modulation was then accomplished using an EG&G 5209 lock-in amplifier. Magnetic field control, data digitizing, and storage were achieved by means of a Stanford Research System SR 245 A/D converter and a personal computer. The magnetic field was independently calibrated with a Bruker ER 035M Gaussmeter. For temperature-dependent measurements between 80 and 293 K, a quartz dewar using nitrogen gas flow was inserted into the microwave resonator. The temperature was measured with a copper−constantan thermocouple above the sample. Typical spectral parameters were 2 mW of incident microwave power, and the magnetic field modulation amplitude was 0.05 mT.

**Calculation Methods.** *Simulation of Spin Dynamics.* Each antenna complex with $N$ pigments was considered as an array of $N$ variables, each variable with a value 1 (if ionized) or 0. The initial distribution of holes was assigned randomly, with the probability of $\chi$ for each BChl to be oxidized. At each $t$th time step, the probability $P_j$ of each hole at the $j$th site to move to the adjacent $(j-1)$th or $(j+1)$th cite was considered. The probability $P_j$ is

$$P_j = \Delta t\, k_{ET} \tag{1}$$

where $\Delta t$ is the length of the time increment and $k_{ET}$ is the electron transfer rate constant. $k_{ET}$ was calculated from other physical quantities using the Marcus expression[25]

$$k_{ET} = 4^2/h\,(4\lambda k_B T)^{-1/2}\, V^2 \exp\{-(\Delta G + \lambda)^2/(4\lambda k_B T)\} \tag{2}$$

where $\lambda$ is the reorganization energy, $\Delta G$ is the free energy change in the reaction, $V$ is the electronic matrix transfer element, $h$ is Plank's constant, $k_B$ is the Boltzmann constant, and $T$ is the temperature. The value of $\Delta t$ was chosen small enough so that $P_j$ never exceeded 0.1 such that the probability of the double transfer during $\Delta t$ can be neglected. Then, the random numbers $r$ were generated, $0 < r < 1$, and the hole transfer was supposed to occur if $r < P_j$. The hole trajectories were calculated for a time period long enough for the slowest relaxation function to decay. For the 0.35 mT wide spectrum, this time was estimated to be 150 ns.

The spin exchange is simulated by exchanging the positions of two adjacent holes. In this work, we considered only two limiting cases, either no exchange or a strong exchange. The latter means that for any time interval $\Delta t$ the probability of exchange is one-half. Below, we shall discuss what the condition of "fast exchange" means for our simulations. Conservation of spin values during the simulation requires the spin lattice relaxation time $T_1 \gg 150$ ns, which is probably true.

In calculating the probabilities of hole transfer using eqs 1 and 2, the repulsion among holes was considered. In our method, without repulsion, $\Delta G$ in eq 2 would always be equal to zero. We calculated $\Delta G$ by considering the Coulombic potential of hole−hole repulsion. The point charge approximation was used for holes, with the effective dielectric constant, $\epsilon$, varied as a parameter. We also excluded doubly oxidized BChls by assigning zero probability for electron transfer to any BChl molecule that had already been oxidized.

**EPR Spectrum Calculation.** A straightforward Monte Carlo approach to the problem would have been to simulate a large number of antennae with various resonance frequencies at every BChl. Suppose that to have a sufficiently smooth Gaussian frequency distribution for one BChl, $M$ randomly distributed resonance frequencies are necessary. For a ring of 32 BChls simulating $M$,[32] various combinations of resonance frequencies would be required. Therefore, a method that utilizes the properties of Gaussian frequency distribution without explicit simulation of various combinations of resonance frequencies would be preferable. Below, we describe such a method, developed especially for use with the random walk simulations of spin dynamics. This method allows incorporation of spin−spin interactions as far as they are reflected in the simulated spin trajectories.

Following Anderson[26] and Kubo,[27] the resonance frequency experienced by a spin, $\omega(t)$, is considered to be a random process. Therefore, the spin phase angle, $\theta(t)$, is also a random variable. The EPR spectrum is the Fourier transform of the

relaxation function, $\phi(t)$, which represents the decay of the transverse polarization in the rotating frame[28]

$$\phi(t) = \langle\theta(t)\theta(0)^*\rangle/|\theta(0)|^2 \quad (3)$$

where the braces mean the ensemble average of the random process. Assume that the heterogeneous distribution of resonance frequencies is Gaussian and coincides with the normalized EPR spectrum of the monomeric $BChl^+$ cation. In the coordinate system rotating with the central frequency of the distribution (i.e., in the rotating frame), the distribution is

$$P_{mono}(\omega) = \frac{1}{\sqrt{2\pi}\sigma_\omega} \exp\{-\omega^2/2{\sigma_\omega}^2\} \quad (4)$$

where $\sigma_\omega$ is the standard deviation, equal in magnetic field units to 0.68 mT. As discussed above, each simulated spin executes transitions between $N$ sites as the result of the electron transfer and exchange processes, where $N$ is the number of BChls in a single antenna complex. At each $n$th site, the spin likely possesses a different resonance frequency. We assume that every simulated trajectory, $n(t)$, corresponds to a large number of spins, all moving in the same manner but experiencing different combinations of the resonance frequencies. These spins constitute the ensemble, whereas the combinations of the resonance frequencies represent the realizations of the $N$-dimensional random variable with distribution

$$P(\omega_1,\omega_2...\omega_N) = P_{mono}(\omega_1) \cdot P_{mono}(\omega_2) \cdot ... \cdot P_{mono}(\omega_N) \quad (5)$$

Following Kubo,[28] a distribution function, $F(\theta,t)$, of the phase angles, $\theta$, of such an ensemble is considered in the rotating frame. At time zero, $F(\theta,0) = \delta(0)$. The time development of $F(\theta,t)$ is the function of the corresponding trajectory, $n(t)$, which is considered a nonrandom function. During the first time interval, $0 < t < t_1$, the spins of the ensemble stay on the BChl number $n_1$. The distribution of the resonant frequencies, $\omega_1$, in the ensemble is static during this time and equal to $P_{mono}(\omega_1)$. For any static heterogeneous frequency distribution $P(\omega)$, the corresponding phase distribution function $f(\theta,t)$ develops in time as

$$f(\theta,t) = \frac{1}{t} P(\theta/t) \quad (6)$$

As follows from eq 6 for the Gaussian distribution $P_{mono}(\omega_1)$, the corresponding phase distribution function $f(\theta,t)$ is also Gaussian. Therefore, at $t = t_1$, the distribution of phases in the ensemble is

$$F(\theta,t_1) = f_1(\theta,t_1) = \frac{1}{\sqrt{2\pi D_1}} \exp\{-\theta^2/2D_1\} \quad (7)$$

where $D_1$, the variance, is expressed as

$$D_1 = (\sigma_\omega t_1)^2 \quad (8)$$

A subensemble of spins, which is experienced in the first time interval $0 < t < t_1$ and resonance frequencies in some interval $\omega_k < \omega < \omega_k + d\omega_k$, is considered. At $t = t_1$, the phase angles, $\theta$, of this subensemble are distributed in the range $\theta_k < \theta < \theta_k + d\theta_k$, where $\theta_k = \omega_k t_1$ and $d\theta_k = d\omega_k \cdot t_1$. At $t = t_1$, the trajectory $n(t)$ changes from $n_1$ to $n_2$. Because the distributions $P(\omega_1)$ and $P(\omega_2)$ are independent, after $t_1$, this subensemble experiences resonant frequencies in the whole range of $P_{mono}(\omega_2)$. By the time $t_2$, the phase distribution function of the subensemble, $f_2(\theta - \theta_k,t_2)$, is the Gaussian function with the variance of $D_2 = \{\sigma_\omega \cdot (t_2 - t_1)\}^2$. Integration over all subensembles gives the phase distribution function for all spins at $t_2$

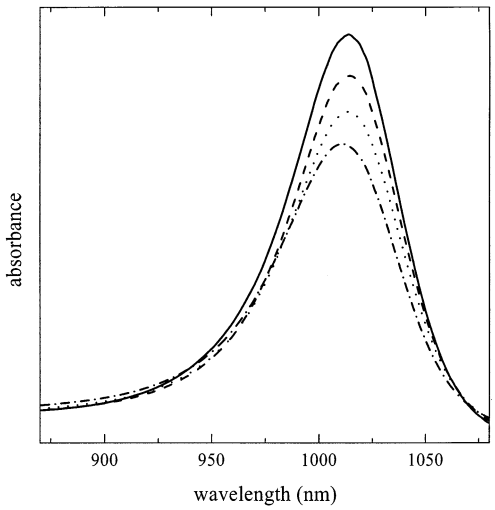


**Figure 1.** Optical absorption spectra of the photosynthetic membranes of *R. viridis* in the spectral region of the $Q_Y$ band. The fractions of the oxidized BChls, $\chi$, are 0, 0.1, 0.18, and 0.27.

$$F(\theta,t_2) = \int f_2(\theta - \theta_k,t_2)\, f_1(\theta,t_1)\, d\theta_k \quad (9)$$

Equation 9 is the convolution of two Gaussian functions, which again yields a Gaussian function with the variance

$$D(t_2) = D_1 + D_2 = {\sigma_\omega}^2 \{{t_1}^2 + (t_2 - t_1)^2\} \quad (10)$$

In general, when the trajectory is at $n^J$, for any subensemble $d\theta^1\, d\theta_2...d\theta_{J-1}\, d\theta_{J+1}...d\theta_N$, the phase distribution function of the subensemble, $f_J(\theta,t)$, is Gaussian. Its variance is proportional to the square of the total time that this trajectory has stayed at $n_J$. By integrating over all subensembles, we find that $F(\theta,t)$ is the Gaussian function with the variance

$$D(t) = {\sigma_\omega}^2 \sum_{n=1}^{N} {\tau_n}^2 \quad (11)$$

where $\tau_n$ is the total time that the hole trajectory has stayed at site $n$ during the time interval from 0 to $t$. For a Gaussian phase distribution function $F(\theta,t)$ with the variance $D(t)$, the relaxation function is[28]

$$\phi(t) = \exp\{-0.5D(t)\} \quad (12)$$

Thus, for each trajectory, $\phi(t)$ can be calculated from eqs 11 and 12, and the corresponding EPR spectrum is the Fourier transform of $\phi(t)$. The spectra from all simulated trajectories were added to yield the final averaged EPR spectrum. In the case of a very fast electron transfer among $N$ molecules, $\tau_n = t/N$; therefore, $D(t) = t^2{\sigma_\omega}^2/N$, and it is easy to show that $\Delta H = \sigma_\omega/N^{1/2}$. As expected, for the trajectories simulated without any spin−spin interactions, the results obtained by using the above method were identical with those obtained by using the Kubo−Anderson method with Markovian modulation,[26,27] reported previously.[24]

## Results and Discussion

**Optical Spectroscopy.** The near-IR absorption lines of the membrane-bound light-harvesting complexes from *B. viridis* are presented in Figure 1. The spectra are taken from the samples

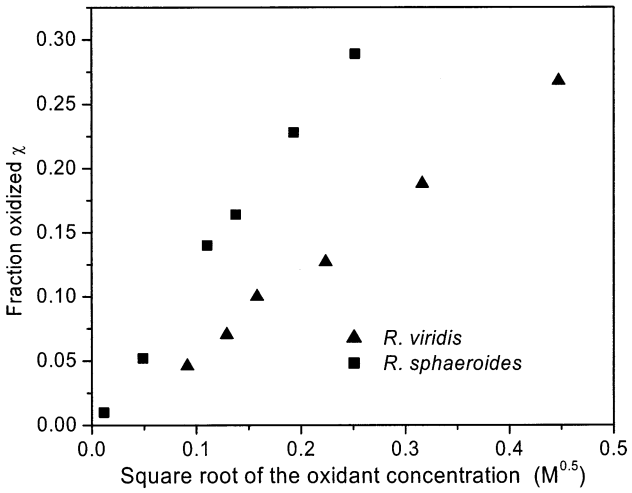


**Figure 2.** Fraction of the oxidized BChls, $\chi$, vs the ferricyanide concentration in the sample. The optical densities in the absorption maximum before oxidation were 25 $cm^{-1}$.

with different fractions, $\chi$, of the BChls oxidized by the different oxidant concentrations. Absorption spectra of the oxidized, detergent-isolated LH1 complexes from *R. sphaeroides* have been presented previously.[24] The major effect of the oxidation is the reduction of the peak intensity. We used the reduction of the amplitude of the antenna peaks as a measure of $\chi$. Because the form of the peak did not change significantly with oxidation and no other pigments are known to absorb at these wavelengths, we can assume that the amplitude of the peak is proportional to the number of neutral BChl molecules. That the antennae oxidized with ferricyanide could be reduced by adding sodium ascorbate was shown previously.[17] We also reduced oxidized LH1 complexes from *R. sphaeroides* except we used sodium ferrocyanide.

Consider the approximate equilibrium equation for the oxidation reaction, where concentrations stand for activities

$$\frac{[\mathrm{BChl}^+][\mathrm{Fe}^{2+}]}{[\mathrm{BChl}][\mathrm{Fe}^{3+}]} = K_{\mathrm{EQ}} \tag{13}$$

where $K_{EQ}$ is the equilibrium constant and $[Fe^{2+}]$ and $[Fe^{3+}]$ are the concentrations of the ferrocyanide and ferricyanide ions, respectively. Assuming that the antenna BChls are the most abundant reducible substance in the solution, we get

$$[\mathrm{BChl}^+] = [\mathrm{Fe}^{2+}] \tag{14}$$

When ferricyanide is in excess and $\chi$ is small, then

$$[\mathrm{Fe}^{3+}] \approx [\mathrm{Fe}^{3+}]_0 \tag{15}$$

$$[\mathrm{BChl}] \approx [\mathrm{BChl}]_0 \tag{16}$$

where $[Fe^{3+}]_0$ is the added amount of the oxidant and $[BChl]_0$ is the BChl concentration before the oxidation. From eqs 13−16, it follows that

$$\chi^2 \equiv [\mathrm{BChl}^+]^2/[\mathrm{BChl}]_0^{\,2} \approx K_{\mathrm{EQ}}[\mathrm{Fe}^{3+}]_0/[\mathrm{BChl}]_0 = \mathrm{const} \cdot [\mathrm{Fe}^{3+}]_0 \tag{17}$$

Figure 2 presents the dependence of the optically determined $\chi$ on the square root of the concentration of the oxidant for the samples from *B. viridis* and *R. sphaeroides*. The observed dependence is approximately linear, in agreement with eq 17. This indicates that the system oxidation behaves as an equilibrium process. The nonlinear dependence of $\chi$ on the ferricyanide concentration was observed by Gingras and Picorel (1990) who interpreted the oxidation process as a binding isotherm. The extinction coefficients in the absorption maximum of the $Q_Y$ band for both BChl*a* and BChl*b* were reported[29,30] to be approximately 100 $mM^{-1}$ $cm^{-1}$. By approximating the dependencies in Figure 2 with straight lines, we obtain the estimates of $K_{EQ}$ values of $0.9 \times 10^{-4}$ and $3.6 \times 10^{-4}$ for *B. viridis* and *R. sphaeroides*, respectively. From these values, the differences of the standard oxidation potentials, $\Delta E^0$, between BChls and ferrocyanide can be calculated as

$$\Delta E^0 = -k_{\mathrm{B}}T \ln(K_{\mathrm{EQ}}) \tag{18}$$

We found $\Delta E^0$ to be 0.23 and 0.20 V for the samples of *B. viridis* and *R. sphaeroides*, respectively. Interpreting the oxidation as bleaching of optical dimers instead of monomers would decrease the slope of Figure 2 by two and would add 0.036 V to each of the two oxidation potentials determined by eq 18. For ferrocyanide in 0.01 M Tris buffer, the standard oxidation potential vs NHE is about 0.41.[31] Thus, for the antennae of *B. viridis* and *R. sphaeroides*, the estimated oxidation potentials are 0.64 and 0.61 vs NHE, respectively. Previously, Picorel et al.[17] reported the midpoint redox potential of chromatophores from *R. sphaeroides* to be 0.55. The difference may be attributed to different growth and separation conditions, as well as the complexity of the system, in which the equilibrium properties may not be easily measured. For additional comparison, the oxidation potentials of RCs are reported to be around 0.49.[32−35] Our values of 0.64 and 0.61 are higher by 5 to 7 $k_BT$ (at room temperature), which helps to prevent the oxidation of LH1 in vivo.

**EPR Measurements.** The line shapes of the measured EPR spectra from *R. sphaeroides* are intermediate between Gaussian and Lorentzian. Good fits to these spectra have been obtained by using the convolution of the Gaussian and Lorentzian line shape or EPR lines simulated by using the method after Tang et al.[36] or the method described in this paper. Spectra from *B. viridis* can be fitted equally well by using the Gaussian or the simulated line for the narrow component. However, for fitting the wings of the spectral line, a broader Gaussian component must be added, which probably represents the EPR signal from the oxidized RC. To obtain the best fit, we needed one narrow (about 0.4 mT) and two broad Gaussian components with widths of 0.95 and 1.3 mT, as shown in Figure 3. Unclear is why the 1.3 mT wide component, corresponding to the monomeric BChl cation, is present in the spectra. The spectra were fitted by appropriate choice of the amplitudes of all three components and the width of the narrow component. Below, we address only the narrow component of the EPR spectra from *B. viridis*.

The dependences of the spectral area of the integrated EPR spectrum, $S_{EPR}$, on $\chi$ for three different sets of measurements are presented in Figure 4 (in relative units). We performed room temperature measurements of $S_{EPR}$ for *R. sphaeroides* and *B. viridis* and a set of low temperature measurements of $S_{EPR}$ for *R. sphaeroides*. The low temperature EPR setup is more sensitive than the room temperature setup. For the sample with $\chi = 0.003$, the value of $\chi$ was calculated from the oxidant concentration using eq 17. Figure 4 shows that $S_{EPR}$ linearly depends on $\chi$ in each set of measurements. The values of $S_{EPR}$ from different sets cannot be compared because of different experimental conditions. Similar low temperature measurements were also reported previously,[24] where linear dependence was observed only for small values of $\chi$. In the earlier work, likely

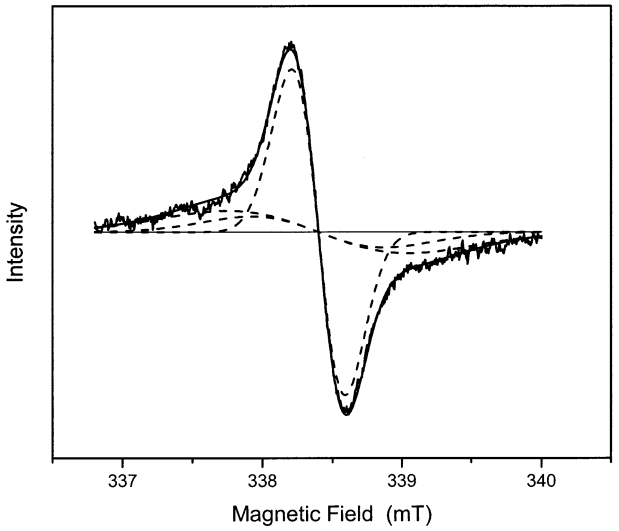


**Figure 3.** EPR spectrum of the oxidized photosynthetic membranes from *B. viridis* ($\chi = 0.27$) and its fit (solid line) with the sum of three Gaussian lines with the widths of 1.3, 0.95, and 0.36 mT (dashed lines).

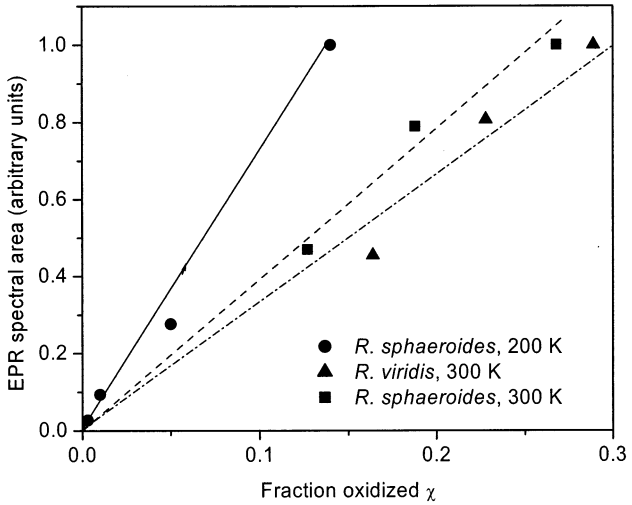


**Figure 4.** Measured EPR spectral intensity vs the fraction oxidized, $\chi$.

some irreversible oxidation occurred. In this work, extra care was taken to measure the EPR spectra immediately after the oxidation.

We now consider the origin of the observed EPR line. We assume that the line originates from antenna complexes where some BChls have been reversibly oxidized to form $BChl^+$ radical cations. We also assume that since the oxidation is reversible, the positive charges can diffuse among the pigments of the same antenna complex. There are several arguments in favor of these assumptions. (i) The EPR line intensity is proportional to $\chi$. (ii) The same narrow EPR line was observed after oxidation of the antenna complexes of *R. sphaeroides* by adding the 0.1 M solution of cerium ammonium nitrate. Therefore, the EPR spectrum is not associated with the particular oxidant. (iii) Upon lowering the temperature of the sample, the EPR line width gradually increases from about 0.4 to 1.36 mT.[24] This is the feature of the temperature-dependent dynamic line narrowing process, which involves several (at least $\{1.36/0.4\}^2 = 11$) interchanging spin configurations. All other mechanisms except the hole diffusion are not capable of reducing the line by 0.8 mT at room temperature.

The EPR line width, $\Delta H$, measured at room temperature for different $\chi$ values, is presented in Figure 5. $\Delta H$ is equal to 0.45

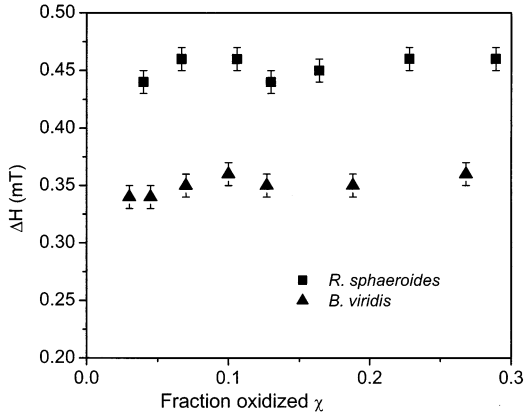


**Figure 5.** Measured EPR line width at room temperature vs the fraction oxidized, $\chi$.

and $0.35 \pm 0.01$ mT for *R. sphaeroides* and *B. viridis*, respectively. The error bars show the spread of the $\Delta H$ values obtained in separate measurements of the same sample. In addition, our fitting method may produce some systematic mistake, which is probably bigger for small values of $\chi$, when the signal from LH1 is weak as compared to that from RC. Figure 5 shows that $\Delta H$ does not depend on $\chi$ for both species within the available range of $\chi$ and the precision of our experiments. Independence of $\Delta H$ on $\chi$ is not easy to understand unless we assume the complete delocalization of the holes over less than the total number of the BChls of the LH1 complex. Below, we show the results of simulations, which attempt to explain these observations with a rate limitation, not a size limitation.

The observed difference of $\Delta H$ in the two types of samples may be caused either by the difference of the properties of the two species in vivo or by the difference in sample preparations. Previous EPR studies of the oxidized LH1 by Picorel et al.[17] showed that the $\Delta H$ increases after separation of LH1. They found $\Delta H$ in the photosynthetic membranes from *R. sphaeroides* and *R. rubrum* to be 0.37 and 0.38 mT, respectively, which are close to the value of 0.35 mT that we measured in the photosynthetic membranes from *B. viridis*. Comparison of these results with $\Delta H$ of 0.45 mT, which we measured in the separated LH1 complexes from *R. sphaeroides*, suggests that this value is also the result of the treatment. There may be two major reasons for this increase: (i) any kind of structural changes including aggregation size and/or distributions of aggregation sizes of the LH1 complex itself; (ii) interaction with the water molecules and ions on the surface of the separated complexes. In the former case, the system is heterogeneous and simulations must consider heterogeneity. The latter can be simulated using the present homogeneous model with increased reorganization energy.

**Simulated EPR Spectra.** To understand better the possible mechanisms of the line narrowing, computer simulations have been preformed for spin dynamics in the oxidized antenna. We assume that the EPR line originates from the LH1 complexes with intact ringlike structure. That the LH1 complexes are likely more monodispersed in size in the membrane preparations as compared to the detergent-isolated preparations is not taken into account and is not critical for explaining the independence of EPR line width to the fraction of BChls oxidized. Also, whether the ringlike structure is open or closed makes little difference.[36] We used two different models, one in which the coupling occurs only between nearest neighbors and the other with additional coupling between next-to-nearest neighbors. The justification for the second model is the analogy with the RC, where both

parts of the special pair primary donor (a dimer of BChls) are highly coupled to the acceptor.[37,38]

We now consider weakly oxidized antennae with low $\chi$, where the probability of having two holes in one LH1 complex is low. Here, $\Delta H$ depends only on the ET rate constant, $k_{ET}$. Having simulated such a system with the nearest neighbor coupling assumption, we found that $k_{ET}$ was equal to $9 \times 10^8$ $s^{-1}$ for the membrane-bound complexes of *B. viridis*. This value agrees with the rate constant of $10^9$ $s^{-1}$ suggested for proteins by Moser et al.[20] and for α-helixes by Winkler et al.[21] for the center-to-center distance of 1 nm. Similar values of the rate constants would be obtained for the line widths of 0.37 and 0.38 mT, which were measured by Picorel et al.[17] in the membrane-bound LH1 complexes from *R. sphaeroides* and *R. rubrum*, respectively. Assuming that the separated LH1 complexes from *R. sphaeroides* are homogeneous, $k_{ET}$ in those complexes is $4 \times 10^8$ $s^{-1}$.

At low $\chi$ in homogeneous samples, $\Delta G$ is equal to zero, since there is no repulsion. As seen from eq 2, when $\Delta G = 0$, $k_{ET}$ depends on two unknown parameters, $\lambda$ and $V$. One of them, for example, $\lambda$, can be arbitrarily assigned and then $V$ can be determined from $k_{ET}$. For high $\chi$, when holes interact with each other, $\Delta G$ is in general nonzero. Hence, the value of $\lambda$ may not be chosen arbitrarily. However, our calculations showed that the choice of $\lambda$ in the range of 0.1−0.3 eV did not significantly alter the results of simulations with $\chi$ as high as 0.4. Thus, we chose the value of $\lambda$ to be 0.1 eV by analogy with the RC.[39,40] With this choice, the value of $V$ for *B. viridis* ($k_{ET} = 9 \times 10^8$ $s^{-1}$) is 0.21 meV. For detergent-isolated, reconstituted LH1 complexes from *R. sphaeroides*, assuming that the matrix element is the same, $\lambda$ is equal to 0.25 eV. We want to stress that these values of $V$ and $\lambda$ are only reasonable estimations since they cannot be unequivocally determined from the room temperature EPR spectra alone.

Applying the nonnearest neighbor coupling model to the 0.35 mT wide spectra from the membrane-bound complexes from *B. viridis*, we find the value of $k_{ET}$ equal to $2 \times 10^8$ $s^{-1}$. The 0.45 mT wide spectra of the detergent-isolated LH1 complexes from *R. sphaeroides*, if they are homogeneous, correspond to $k_{ET}$ of $1.1 \times 10^8$ $s^{-1}$. The smaller value of the rate constant is required for this model because, not restricted to nearest neighbor transfer, more possibilities for hole transitions exist.

By substituting the values for $V$ and $\lambda$ obtained from the low $\chi$ simulations, we simulated the spin dynamics in antennae with $\chi$ varying from 0 to 0.4. We also varied $\epsilon$. To elucidate the role of the exchange interaction, we simulated two limiting cases of exchange, the strong exchange with 50% probability every time when two holes appear at adjacent BChls and no exchange at all. Below, we present only the results corresponding to the membrane-bound LH1 complexes from *B. viridis* since for the other systems we obtained similar results. The values of $\Delta H$ calculated by using nearest-neighbor model without exchange are shown in Figure 6. Contrary to expectations, we obtained a strong broadening of the EPR spectra with increasing $\chi$. This is because multiple holes in one complex hamper motions of each other. Without Heisenberg spin exchange, two holes cannot exchange their positions, so each hole is "trapped" between two others. Hence, the number of BChls that each hole can access decreases with increasing $\chi$. The line widths depend on $\epsilon$ because this parameter controls the repulsion, and stronger repulsion increases the hampering. The values of $\Delta H$, calculated with the same nearest neighbor model but with strong exchange, are presented in Figure 7 and show a completely different dependence on $\chi$. Here at small values of $\chi$, the spectrum slightly

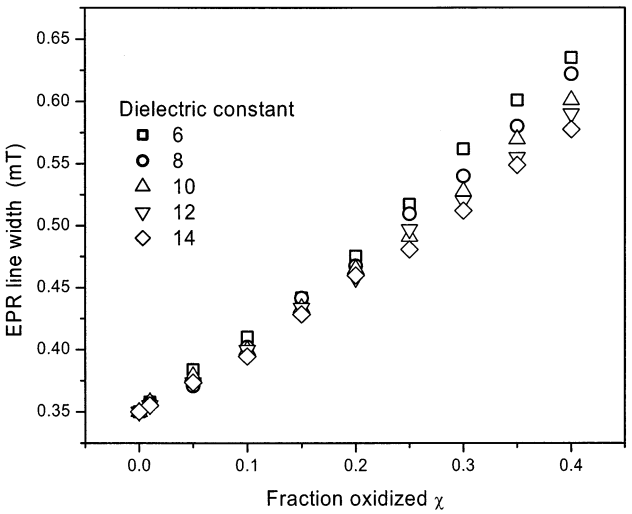


**Figure 6.** Calculated EPR line width vs the fraction oxidized, $\chi$, for *B. viridis*, nearest neighbor coupling model without exchange.

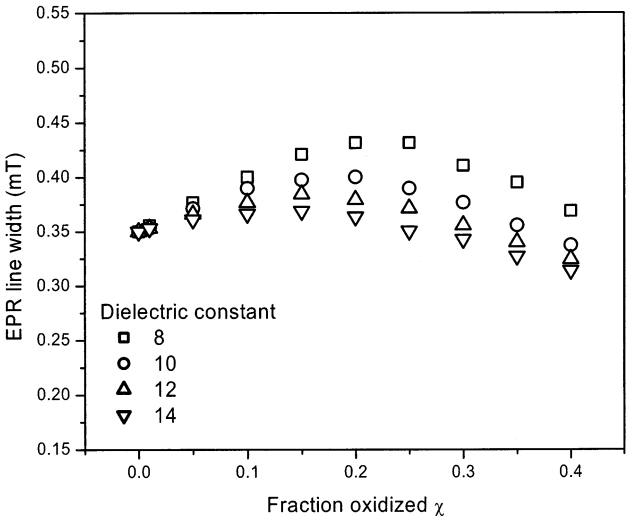


**Figure 7.** Calculated EPR line width vs the fraction oxidized, $\chi$, for *B. viridis*, nearest neighbor coupling model with exchange.

broadens, but with further increase of $\chi$, it starts narrowing. The reason for the narrowing is the growing rate of exchange. The line width depends on $\epsilon$ because electrostatic repulsion hampers holes from interacting with each other. For the values of $\epsilon$ of about 12, only a weak dependence on $\chi$ is observed in the calculated range. Exchange interaction contributes to the line narrowing because (i) it is an additional narrowing mechanism by itself; (ii) it allows the holes to exchange their positions and avoid hampering so that every hole can access all BChls of the ring. With increasing $k_{ET}$, the first reason becomes less important, since electron transfer becomes an efficient narrowing mechanism by itself; however, the second reason becomes more important because of the increasing range of LH1 that each hole can access if there is no hampering.

The results of the nonnearest neighbor coupling model with exchange are presented in Figure 8. They depend less on $\chi$ and $\epsilon$, although the required value of $\epsilon$ is larger. With $\epsilon$ equal to 18, the dependencies of $\Delta H$ on $\chi$ are nearly flat. The reason is that with nonnearest coupling the holes can exchange their positions without Heisenberg exchange, just "bypassing" each other. Therefore, the dynamics depends less on the exchange rate and hence on $\chi$. However, exchange is necessary here, too. We need to assume a high value of $\epsilon$ in order to explain the $\Delta H$ independence of $\chi$. The value of $\epsilon$ controls the repulsion of

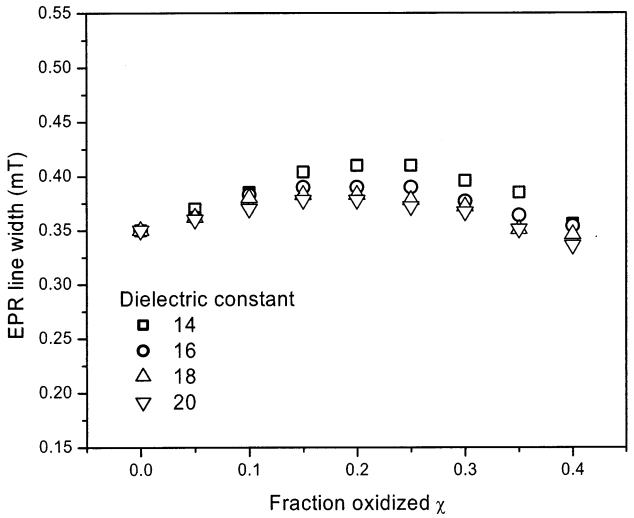


**Figure 8.** Calculated EPR line width vs the fraction oxidized, $\chi$, for *B. viridis*, nonnearest neighbor coupling model with exchange.

holes and thus the rates of their interactions. Our values of 12 and 18 for the two discussed models agree with theoretical and experimental results for proteins, which indicate that for the interaction of charged particles, the effective dielectric constant is in the range of 10−20.[41−47]

In our calculations, we neglected the dipole−dipole interaction, which may be an additional source of line broadening. We believe that due to repulsion, the holes spend only a short time at the adjacent BChls such that most of the time the distances of hole-to-hole separations are large. This behavior reduces the dipole−dipole interaction, whereas the exchange interaction is assumed strong enough to occur during the short periods of time, when the holes approach each other.

The assumption of strong exchange is necessary for the simulations in order that the line width be as independent of $\chi$ as possible. In this work, exchange occurs every time two holes appear at the adjacent BChls during the time interval, $\Delta t$, that they reside close to each other. Therefore, the strong exchange condition in our simulations means

$$k_{EX} \gg 1/\Delta t \tag{19}$$

where $k_{EX}$ is the pseudo-first-order exchange rate constant for two adjacent spins. In our calculation, the time increment, $\Delta t$, is made small enough that the probability of the electron transfer during that time is low, namely, not more than 0.1. Thus,

$$\Delta t < 0.1/k_{ET} \approx 0.1 \text{ ns} \tag{20}$$

Analysis of the results of simulation supported the condition ( eq 20) since decreasing $\Delta t$ less than 0.1 ns did not result in any further decrease of the simulated line width. From eqs 19 and 20, it follows that "strong exchange" in this work means

$$k_{EX} \gg 10k_{ET} \tag{21}$$

For through-space exchange interactions, Closs et al.[48] suggested the following estimation (in frequency units, $s^{-1}$)

$$k_{EX} \approx 10^{12} \exp\{-10.6(R - Ro)\} \tag{22}$$

where $(R - Ro)$ is the edge-to-edge distance in nanometers. We assume that adjacent BChls in LH1 are nearly parallel, with the distance between the two planes approximately 0.45 nm as estimated from the coordinates of the model of Hu and Schulten.[19] The radius of a nonbonded carbon atom is equal to 0.18 nm,[49] and *Ro* may be estimated as twice this distance. Thus, $(R - Ro)$ is equal to 0.09 nm, and the estimated value for $k_{EX}$ is $4 \times 10^{11}$ $s^{-1}$, which is more than necessary to satisfy eq 21.

## Conclusion

Experimentally, we found that the EPR spectra of the oxidized LH1 complexes do not depend on the fraction of the BChls oxidized at room temperature. These spectra can be simulated by assuming a random walk hole movement in a ringlike structure of 32 BChl molecules. The electron transfer rate constants are of the order of $10^8-10^9$ $s^{-1}$. This model also attempts a reasonable explanation for the line width independence of the fraction BChls oxidized if a strong exchange interaction between adjacent spins is assumed.

The hypothesis used in this work is that $\Delta H$ is rate-limited because the observed or calculated line width is larger than the full delocalization limit, characterized by the $1/N^{1/2}$ rule assuming $N = \sim 32$. However, this model does not perfectly explain the experimental behavior, which seems to be completely independent of the observed experimental $\Delta H$ on $\chi$, suggesting some type of size limitation. Because the dynamical behavior of a spin inevitably depends on the presence of other nearby spins, any rate-limited EPR spectrum must somehow depend on $\chi$, even if only slightly as in Figure 8. The other possibility to explain the deviation from $1/N^{1/2}$ rule is that some BChls have higher oxidation potentials, $E^{OX}$, than others, thus being less accessible for holes. However, these "high" BChls may still be oxidized at larger $\chi$ unless their $E^{OX}$ is higher by several *kT*. Strict independence of $\chi$ is possible only in the systems where all holes are delocalized (by means of fast electron transfer and exchange) over a constant number of BChls; other BChls, if present, must be essentially inaccessible to the unpaired spins. Presently, we cannot explain or exclude the possibility of such high differences of $E^{OX}$ in LH1 without further study.

**Acknowledgment.** We gratefully acknowledge support from the U. S. Department of Energy, Office of Basic Energy Sciences, and Division of Chemical Sciences Contract DE-FG02-96ER14675.

## References and Notes

(1) Fleming, G. R.; vanGrondelle, R. *Curr. Opin. Struct. Biol.* **1997**, *7*, 738.
(2) Sundstrom, V.; Pullerits, T.; van Grondelle, R. *J. Phys. Chem. B* **1999**, *103*, 2327.
(3) Vangrondelle, R. *Biochim. Biophys. Acta* **1985**, *811*, 147.
(4) Vangrondelle, R.; Dekker, J. P.; Gillbro, T.; Sundstrom, V. *Biochim. Biophys. Acta-Bioenerg.* **1994**, *1187*, 1.
(5) Pullerits, T.; Sundstrom, V. *Acc. Chem. Res.* **1996**, *29*, 381.
(6) Engelhardt, H.; Engel, A.; Baumeister, W. *Proc. Natl. Acad. Sci. U.S.A.* **1986**, *83*, 8972.
(7) Ikeda-Yamasaki, I.; Odahara, T.; Mitsuoka, K.; Fujiyoshi, Y.; Murata, K. *FEBS Lett.* **1998**, *425*, 505.
(8) Miller, K. R. *Nature* **1982**, *300*, 53.
(9) Stahlberg, H.; Dubochet, J.; Vogel, H.; Ghosh, R. *J. Mol. Biol.* **1998**, *282*, 819.
(10) Stark, W.; Kuhlbrandt, W.; Wildhaber, I.; Wehrli, E.; Muhlethaler, K. *EMBO J.* **1984**, *3*, 777.
(11) Walz, T.; Jamieson, S. J.; Bowers, C. M.; Bullough, P. A.; Hunter, C. N. *J. Mol. Biol.* **1998**, *282*, 833.
(12) Warshel, A.; Papazyan, A.; Muegge, I. *J. Biol. Inorg. Chem.* **1997**, *2*, 143.
(13) Jungas, C.; Ranck, J. L.; Rigaud, J. L.; Joliot, P.; Vermeglio, A. *EMBO J.* **1999**, *18*, 534.
(14) Gingras, G.; Picorel, R. *Proc. Natl. Acad. Sci. U.S.A.* **1990**, *87*, 3405.
(15) Gomez, I.; Sieiro, C.; Ramirez, J. M.; Gomezamores, S.; Delcampo, F. F. *FEBS Lett.* **1982**, *144*, 117.

(16) Gomez, I.; Sanchez, A.; Delcampo, F. F. *Physiol. Veg.* **1985**, *23*, 583.
(17) Picorel, R.; Lefebvre, S.; Gingras, G. *Eur. J. Biochem.* **1984**, *142*, 305.
(18) Norris, J. R.; Uphaus, R. A.; Crespi, H. L.; Katz, J. *Proc. Natl. Acad. Sci. U.S.A.* **1971**, *68*, 625.
(19) Hu, X.; Schulten, K. *Biophys. J.* **1998**, *75*, 683.
(20) Moser, C. C.; Keske, J. M.; Warncke, K.; Farid, R. S.; Dutton, P. L. *Nature* **1992**, *355*, 796.
(21) Winkler, J. R.; Di Bilio, A. J.; Farrow, N. A.; Richards, J. H.; Gray, H. B. *Pure Appl. Chem.* **1999**, *71*, 1753.
(22) Seth, J.; Palaniappan, V.; Johnson, T. E.; Prathapan, S.; Lindsey, J. S.; Bocian, D. F. *J. Am. Chem. Soc.* **1994**, *116*, 10578.
(23) Hiraishi, A. *Int. J. Syst. Bacteriol.* **1997**, *47*, 217.
(24) Srivatsan, N.; Weber, S.; Kolbasov, D.; Norris, J. R. *J. Chem. Phys. B* **2002**, in press.
(25) Marcus, R. A.; Sutin, N. *Biochim. Biophys. Acta* **1985**, *811*, 265.
(26) Anderson, P. W. *J. Phys. Soc. Jpn.* **1954**, *9*, 316.
(27) Kubo, R. *J. Phys. Soc. Jpn.* **1954**, *9*, 935.
(28) Kubo, R. A stochastic theory of line shape and relaxation. In *Fluctuation, Relaxation and Resonance in Magnetic Systems*; Ter Haar, D., Ed.; Oliver and Boyd: Edinburgh, 1961.
(29) Oelze, J. *Methods Microbiol.* **1985**, *18*, 257.
(30) Smith, J. H. C.; Benitez, A. Chlorophyll: analysis in plant materials. In *Modern Methods of Plant Analysis*; Paech, K., Tracy, M. V., Eds.; Springer-Verlag: Berlin, 1955; Vol. 4, p 142.
(31) O'Reilly, J. E. *Biochim. Biophys. Acta* **1973**, *292*, 509.
(32) Popov, M. S. Effect of Point Mutations on the Energetics of Photosynthetic Reaction Centers. Ph.D., The University of Chicago, 1996.
(33) Lin, X.; Murchison, H. A.; Nagarajan, V.; Parson, W. W.; Allen, J. P.; Williams, J. C. *Proc. Natl. Acad. Sci. U.S.A.* **1994**, *91*, 10265.
(34) Moss, D. A.; Leonhard, M.; Bauscher, M.; Mantele, W. *FEBS Lett.* **1991**, *283*, 33.
(35) Gao, J. L.; Shopes, R. J.; Wraight, C. A. *Biochim. Biophys. Acta* **1990**, *1015*, 96.
(36) Tang, J.; Dikshit, S. N.; Norris, J. R. *J. Chem. Phys.* **1995**, *103*, 2873.
(37) Kolbasov, D.; Scherz, A. *J. Phys. Chem. B* **2000**, *104*, 1802.
(38) Zhang, L. Y.; Friesner, R. A. *Proc. Natl. Acad. Sci. U.S.A.* **1998**, *95*, 13603.
(39) Warshel, A.; Chu, Z. T.; Parson, W. W. *J. Photochem. Photobiol. A* **1994**, *82*, 123.
(40) Walz, T.; Ghosh, R. *J. Mol. Biol.* **1997**, *265*, 107.
(41) Sham, Y. Y.; Muegge, I.; Warshel, A. *Biophys. J.* **1998**, *74*, 1744.
(42) Rees, D. C. *J. Mol. Biol.* **1980**, *141*, 323.
(43) Svensson, B.; Jonsson, B. *J. Comput. Chem.* **1995**, *16*, 370.
(44) Warshel, A.; Russell, S. T. *Q. Rev. Biophys.* **1984**, *17*, 283.
(45) Olson, M. A.; Reinke, L. T. *Proteins: Struct., Funct., Genet.* **2000**, *38*, 115.
(46) Cory, M. G.; Zerner, M. C. *J. Am. Chem. Soc.* **1996**, *118*, 4148.
(47) Schutz, C. N.; Warshel, A. *Proteins: Struct., Funct., Genet.* **2001**, *44*, 400.
(48) Closs, G. L.; Forbes, M. D. E.; Piotrowiak, P. *J. Am. Chem. Soc.* **1992**, *114*, 3285.
(49) Brooks, B. R.; Bruccoleri, R. E.; Olafson, B. D.; States, D. J.; Swaminathan, S.; Karplus, M. *J. Comput. Chem.* **1983**, *4*, 187.